Astro2020 Science White Paper

Opportunities in Time-domain Stellar Astrophysics with the NASA Near-Earth Object Camera (NEOCam)

Thematic Areas

Primary: Stars and Stellar Evolution

Secondary: Formation and Evolution of Compact Objects

Principal Author

J. Davy Kirkpatrick
(Caltech/IPAC)
davy@ipac.caltech.edu
Phone 626-395-1850

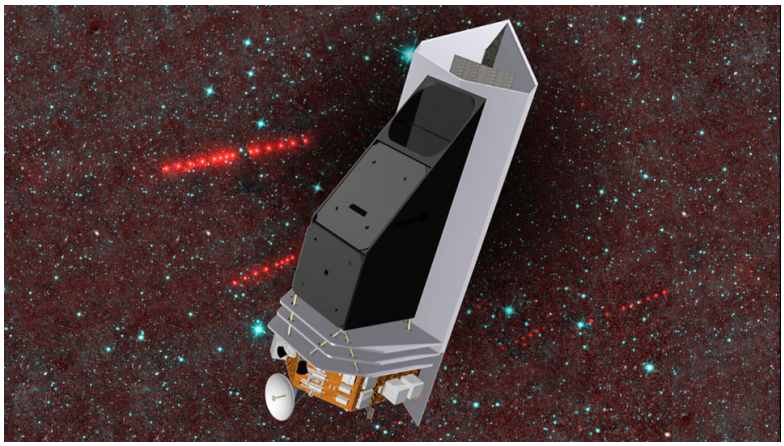

Co-authors

Stanimir A. Metchev (Western U.)
Lynne A. Hillenbrand (Caltech)
Matthew Hankins (Caltech)
Jacob E. Jencson (Caltech)
Kenneth A. Marsh (Caltech/IPAC)
Mansi M. Kasliwal (Caltech)
Kishalay De (Caltech)
Federico Marocco (JPL)
Michael C. Cushing (UToledo)
Edward L. Wright (UCLA)
Mark S. Marley (NASA-Ames)
Roc M. Cutri (Caltech/IPAC)
Amanda K. Mainzer (JPL)

Abstract

The NASA Planetary mission NEOCam will provide invaluable data for the discovery and characterization of cold brown dwarfs, exoplanet analogs exhibiting weather variations, pre-main sequence variables showing sudden mass transfer events, infrared-only transients, and other stellar phenomena. For a relatively small investment, NASA can realize the full potential of NEOCam data for stellar astrophysical research by providing additional data products and transient alerting infrastructure, as described herein.

The NASA Near-Earth Object Camera (NEOCam)

Overview: NEOCam is a NASA Planetary mission, currently in Phase A, whose goal is to discover and characterize asteroids and comets, to assess the hazard to Earth from near-Earth objects, and to study the origin, evolution, and fate of asteroids and comets. NEOCam is a single-instrument, 50cm diameter telescope that will observe in two simultaneous channels, called NC1 and NC2, which cover wavelengths of 4.0-5.2 μm and 6.0-10.0 μm, respectively. There are four Teledyne 2K×2K HgCdTe arrays per channel with 3.00" pixels in each. The entire celestial sphere between ecliptic latitudes of +40° to −40° will continually be mapped over the course of the 5-yr mission, and over 12 yr for the design lifetime.

Cadence: Estimates of on-board overheads and resulting orbit quality are still being refined, but the current data cadence is as follows. The observing pattern consists of a four-peat of a six-position dither (a quick sequence of six images with 28s integration time each) with 2h gaps between each repeat. This four-peat will recur ~13.2d later as long as the 75d visibility window is still open. Afterward, there will be a gap of 215d until the next visibility window opens and the pattern begins again. On average in a typical visibility window, there are ~23 of these six-position dither sequences (a little less than 6 four-peats), ~234 over 5yr, and ~562 over 12yr.

Depth: Each of the six-position dither sequences is expected to have an S/N=5 sensitivity of 65-120 μJy for NC1 and 110-280 μJy for NC2, for low to high zodiacal backgrounds.

Data Products: NEOCam processing will create images and lists of characterized sources from each individual exposure and each stacked six-dither position sequence. It will also create differenced images by subtracting a static reference image, along with a list of characterized transient detections. Because the goal of NEOCam is to provide and characterize moving objects within the solar system, coadd and source extractions over longer timescales are not provided, the one exception being yearly builds to create new static images of the sky (without any source detection or characterization) to use in image differencing.

To realize the full potential of the NEOCam data for astrophysical research, additional data products and alerting infrastructure are needed. For a relatively small investment, NASA can leverage existing NEOCam data to cover a wide range of stellar research, as discussed below.

The Identification of Very Cold Brown Dwarfs

> Critical questions: What is the low-mass cutoff of star formation? Has this process produced brown dwarfs with temperatures comparable to the giant planets of our Solar System?

Cold brown dwarfs are most easily detected between 4 and 5 μm because most of their emission leaks out in an opacity-free zone located amid water, methane, and ammonia absorption bands at shorter and longer wavelengths (Figure 1). Even here, cold brown dwarfs are quite faint, with absolute fluxes of 237 μJy for a 450K Y0 dwarf, 103 μJy for a 350K Y2 dwarf, and 26 μJy for a 250K (Y4?) dwarf (Cushing et al., 2011; Schneider et al. 2015; Kirkpatrick et al. 2019). To detect more of these objects and ones of even colder temperature, large-area searches from space are needed. Both JWST and the Cosmic Dawn Intensity Mapper (Cooray et al. 2016) operate at these wavelengths but cannot cover large swaths of sky.

SPHEREx (Doré et al. 2016, 2018) is all-sky and operates at the correct wavelengths but is not as deep as WISE. Of currently planned or proposed missions, only NEOCam provides the needed sensitivity and sky coverage.

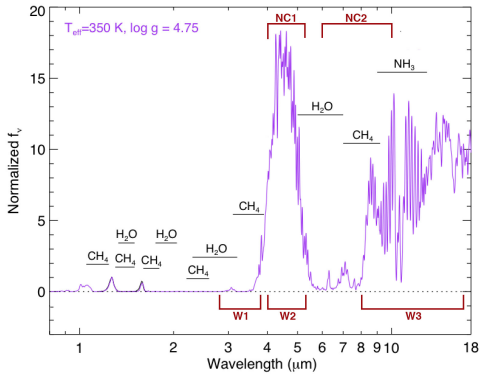

Figure 1: A model brown dwarf spectrum (purple; M. Marley, priv. comm.). Major absorption bands of H_2O, CH_4, and NH_3 are indicated (black). Shown in brown are regions covered by the WISE W1, W2, and W3 bands and regions covered by the NEOCam NC1 and NC2 bands. Discovery and characterization of cold brown dwarfs is most easily done between 4 and 5 μm where most of their flux is emitted.

Recent analysis of the 20-pc brown dwarf sample has shown that the low-mass cutoff of star formation is below 5 M_{Jup} (Kirkpatrick et al. 2019). As Figure 2 illustrates, pushing to lower masses means searching below T_{eff} = 300K. So far, only one such object has been identified – the 250K Y dwarf WISE 0855−0714 (Luhman 2014). Other objects undoubtedly exist (Wright et al. 2016), as this object was identified primarily because of its high motion (8”/yr) and proximity to the Sun (2.3 pc).

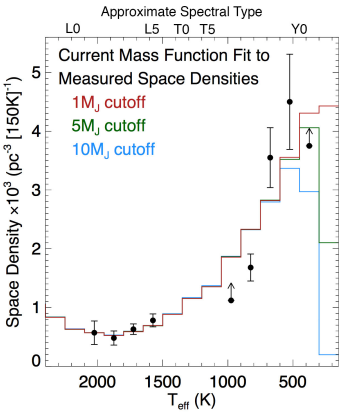

Figure 2: Space density of the (incomplete) 20-pc sample as a function of T_{eff} (black points), adapted from Kirkpatrick et al. (2019). The larger error bars on the rightmost points are caused by the much smaller volumes sampled there. Also plotted are simulations based on various forms of the mass function, for which the power-law of exponent α=0.6 (shown) provides the best fit. This model is illustrated with three different cutoff masses (10, 5, or 1 M_{Jup}). The cutoff mass is best measured by the coldest bin shown, T_{eff} = 150-300K, for which a space density has yet to be measured.

Does NEOCam have the depth needed to find a significant number of objects below T_{eff} = 300K? At S/N = 5, an individual epoch of NEOCam data reaches NC1 ≈ 40 μJy, the full root-of-N improvement not being realized because of confusion. We can probe below this confusion limit, however, by using image differencing, whereby the limiting factor then becomes the lower-level residuals from background subtraction, as determined by the effects of non-isoplanicity and registration errors. Tests on NEOWISE W2 images demonstrate an improvement of 10× over the nominal confusion limit. This means that sensitivities of NC1 ≈ 4 μJy can be achieved with NEOCam.

This potential depth can be realized even for high motion objects by employing a detection technique that is capable of identifying a moving source without knowing in advance its position or proper motion vector. The technique uses a shift-and-add operation on images at multiple epochs to optimize the S/N in a 5D search space consisting of position, proper motion, and parallax. We can thus identify nearby motion objects that satisfy the depth criteria, outlined in Table 2 of Leggett et al. (2019), needed to identify dozens of brown dwarfs below T_{eff} = 300K. This population will provide a robust space density in the coldest bin shown in Figure 2 and will also help answer whether solivagant brown dwarfs exist with T_{eff} values comparable to the giant planets of our Solar System (124 K for Jupiter; Hanel et al. 1981).

NEOCam products needed: NC1 coadds are required for all NEOCam data within a visibility window along with full coadds using all accumulated data. Additionally, novel processing is required to identify and characterize moving detections found in difference images made from these coadds.

Weather Variations in Exoplanet Analogs

Critical questions: How do the atmospheres of brown dwarfs vary? How can this info be used to constrain models of exoplanet atmospheres that have the additional complication of irradiation by a host star?

With convective interiors driving instabilities in their overlying condensate-rich atmospheres (Burrows & Liebert 1993, Robinson & Marley 2014), L and T dwarfs are now known to exhibit photospheric heterogeneities (Metchev et al. 2015). These are observed as rotationally modulated 0.1%-10% photometric variations, and have provided the first indication of weather phenomena on brown dwarfs (Artigau et al. 2009). The spectrophotometric effects increase in contrast toward colder late-T (Metchev et al. 2015) and Y dwarfs (Leggett et al. 2016, Esplin et al. 2016), reaching tens of percent in the mid-infrared for Jupiter (Gelino & Marley 2000; Ge et al. 2019). Long-duration Spitzer monitoring of three variable early-T dwarfs reveals complex and evolving light curves (Apai et al. 2017), likely due to a combination of spots (storms) and planetary-scale longitudinal waves (belts). As seen in Figure 3, such spots and belts compare well to the infrared reflected light morphology of Neptune. The atmospheric structures of colder T and Y dwarfs are expected to be even more similar to those of gas giant planets.

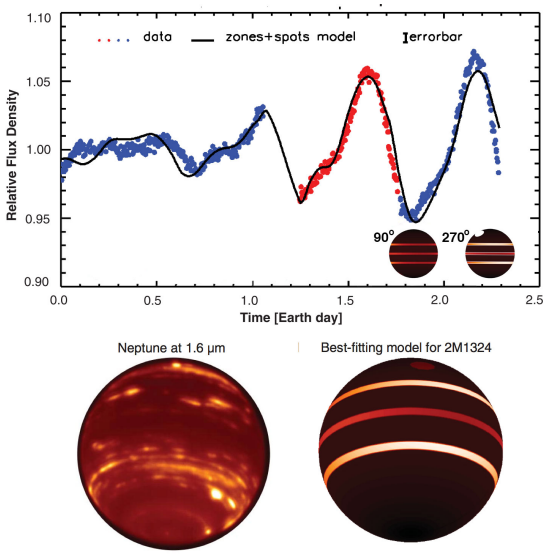

Figure 3, adapted from Apai et al. (2017): (Top panel) The evolving light curve of the transition L/T dwarf 2MASS 1324+6358 observed by Spitzer at 3.6 μm (blue points) and 4.5 μm (red points). The black line represents a model using three sinusoidally modulated bands and a bright spot. The inset at lower right shows the model at two points toward the end of the data sequence. (Bottom panel) The morphology of Neptune's cloud features as seen in near-infrared scattered light compared to the best fitting model for this L/T dwarf. Spots and belts approximate well the reflected light patterns seen on Neptune.

Multi-year monitoring by NEOCam will result in an unbiased large-area survey of photometric variations in brown dwarfs, extending to the coolest, planetary-mass objects. Follow-up observations with other facilities at higher cadence will determine the nature of the variability, and will test the existence of longitudinal belts outside of the early-T range. For example, the change from a spotted to a banded appearance may play a role in the large, unexplained dispersion in spectrophotometric properties across the L-to-T spectral type transition (cf. Zhang & Showman 2014). An assessment of the variability of the coldest brown dwarfs will give the first glimpse into the range of atmospheric dynamical phenomena expected for widely orbiting,

mostly non-irradiated exoplanets around other stars. By simultaneously probing deep atmospheric layers in the nearly opacity-free NC1 band and in the strongly gas-absorbed NC2 band, NEOCam will be sensitive to the presence of clouds across a broad range (~0.1-10 bar) of atmospheric pressures (Morley et al. 2012).

> NEOCam products needed: NC1 and NC2 coadds and extractions are required in each visibility window to create a database against which to search for objects exhibiting variability.

FU Orionis-type Outbursts

> Critical questions: Is the frequency of large-scale episodic accretion in protostars sufficient to explain the current shortfall inferred for disk-to-star mass accumulation? How do we identify more of these events?

Stars form via infall from a slowly rotating hydrostatic core, with the build-up of stellar mass occurring through a combination of direct collapse and rapid accumulation of material from a disk, followed by a late-accretion phase that competes with planet formation in depleting the disk. One problem in this framework is the low luminosities of protostars, implying lower than expected accretion rates. Another problem is the inability to build stellar masses at the measured disk accretion rates on the timescales seen. Our current understanding of stellar mass assembly thus relies on the concept of episodic accretion: punctuated periods of mass accumulation that are 3-4 orders of magnitude larger than seen in typical young accretors.

Hartmann & Kenyon (1996) hypothesized that enhanced accretion occurs more frequently in more massive disks at early protostellar stages, and thus that the rate of so-called FU Ori events should be higher for protostars and lower for optically revealed pre-main sequence stars. Subsequent detailed modeling of instabilities arising in the inner (Bae et al. 2014) or outer disk (Vorobyov & Basu 2015) has produced quantitative predictions concerning the amplitudes, durations, and duty cycles of episodic accretion in young stellar objects. The existing theoretical guidance is that every forming star undergoes ~10-20 of these catastrophic disk instability-driven events in its first 1 Myr of life.

However, empirical support for this paradigm is lacking. Over the past 7 decades, only 13 FU Ori outbursts have been recorded (half in the past decade), with a comparable number of sources identified as “FU Ori-like” based on spectra and photometry indicating a post-outburst state (Reipurth & Aspin 2010; Connelley & Reipurth 2018). The dearth can be explained if the majority of events happens only in the deeply embedded phase and thus detectable only in the near- or mid-infrared. Finding the missing events is a critical test of theory.

With its repeated scanning in the mid-infrared, NEOWISE has already contributed to this field by participating in the identification of the most recently identified FU Ori star, Gaia 17bpi (Hillenbrand et al. 2018). Indeed, the NEOWISE data brought new insight by demonstrating – for the first time – that FU Ori outbursts originate in the mid-infrared and manifest only later in the optical. For Gaia 17bpi, the delay was 1.5 years. The rise times for FU Ori outbursts range from about 100 to about 2000 days, with amplitudes between 3 and 7 magnitudes. The wavelength coverage and cadence of NEOCam are therefore perfect for alerting the community to other, similar events.

NEOCam products needed: Same as in the previous section, with the addition of an alerting infrastructure to quickly inform the community about active transients.

Infrared-only Transients

Critical questions: What is the nature of infrared-only transients that lie in the luminosity gap between novae and supernovae? How do we identify and follow-up additional examples for further study?

The systematic exploration of the dynamic infrared sky is just beginning. The SPIRITS survey (PI: M. Kasliwal), is a large, ongoing search for infrared stellar transients in a sample of 190 nearby galaxies within ~20 Mpc using Spitzer/IRAC at 3.6 and 4.5 μm. This pioneering survey has identified over 2500 strong infrared variables and discovered over 80 explosive transients. The sample spans lower-luminosity events consistent with classical novae, to more luminous events possibly associated with heavily dust-obscured core collapse supernovae, massive stellar mergers, electron-capture explosions of extreme asymptotic giant branch stars, and self-obscuring, giant eruptions of massive evolved stars (Jencson et al. 2019).

In addition, SPIRITS has discovered a new class of infrared transients known as ``SPRITEs'' (Kasliwal et al. 2017) that have no detectable optical counterparts. Lying in the infrared luminosity ``gap'' between novae and supernovae (see Figure 4), SPRITEs have a nature that remains unclear, as no ground-based telescope is currently capable of obtaining spectra. Proposed origins include shocks in molecular clouds driven by the formation of close, massive binaries, the birth of stellar mass black holes in the direct collapse of a massive star in a ``failed supernova'' (Adams et al. 2017), and stellar mergers (Blagorodnova et al. 2017; Metzger et al. 2017) or electron-capture supernovae for which enough dust survives the explosions to completely obscure the optical transient.

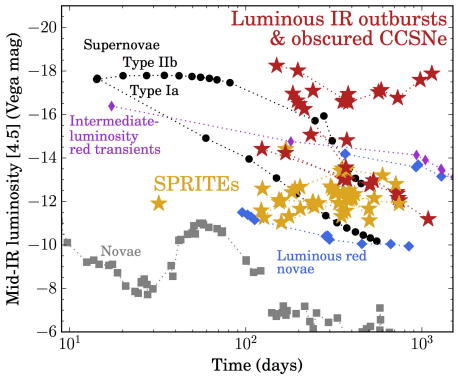

Figure 4: Light curves of SPIRITS transients compared to supernovae (black circles) and classical novae (grey squares). SPRITEs (yellow stars) fall in the luminosity gap between novae and supernovae. The 9 most luminous SPIRITS transients (red stars) include 5 heavily dust obscured core collapse supernovae, a luminous red nova associated with a massive star merger, an intermediate-luminosity red transient associated with a low-energy or electron-capture supernova, and 2 massive evolved stars with multiple dusty outbursts.

NEOCam is shallower than Spitzer/IRAC but can search a much wider area and hence larger volume. NEOcam's 2024 launch provides an overlapping window with JWST. When both observatories are in operation, NEOcam will act as a discovery machine, with JWST providing deep infrared spectroscopic follow-up. Discoveries in NEOcam data are needed along with timely alerts to enable the follow-up necessary to reveal the nature of SPRITEs and similar sources that are so heavily reddened to be inaccessible at shorter wavelengths.

NEOCam products needed: Same as in the previous section

References

Adams, S.M., Kochanek, C.S., Gerke, J.R., et al., 2017, MNRAS, 468, 4968.
Apai, D., Karalidi, T., Marley, M., et al. 2017, Science, 357, 683.
Artigau, É., Bouchard, S., Doyon, R. & Lafrenière, D., 2009, ApJ, 701, 1534.
Bae, J., Hartmann, L., Zhu, Z., & Nelson, R.P., 2014, ApJ, 795, 61.
Blagorodnova, N., Kotak, R., Polshaw, J., et al., 2017, ApJ, 834, 107.
Burrows, A. & Liebert, J., 1993, Rev. Mod. Phys. 65, 301.
Connelley, M.S., & Reipurth, B., 2018, ApJ, 861, 145.
Cooray, A., Bock, J., Burgarella, D., et al., 2016, arXiv, 160205178C.
Cushing, M.C., Kirkpatrick, J.D., Gelino, C.R., et al., 2011, ApJ, 743, 50.
Doré, O., Werner, M.W., Ashby, M., et al., 2016, arXiv, 160607039D.
Doré, O., Werner, M.W., Ashby, M.L.N., et al., 2018, arXiv, 180505489D.
Esplin, T., Luhman, K., Cushing, M., et al. 2016, ApJ, 832, 58.
Ge, H., Zhang, X., Fletcher, L., et al., 2019, AJ, 157, 89.
Gelino, C. & Marley, M., 2000, ASP Conf. Ser., 212, 322.
Hanel, R., Conrath, B., Herath, L., et al., 1981, JGeophysRes, 86, 8705.
Hartmann, L., & Kenyon, S.J., 1996, ARA&A, 34, 207.
Hillenbrand, L.A., Contreras Peña, C., Morrell, S., et al., 2018, ApJ, 869, 146.
Jencson, J.E., Kasliwal, M.M., Adams, S.M., et al., 2019, arXiv, 190100871.
Kasliwal, M.M., Bally, J., Masci, F., et al., 2017, ApJ, 839, 88.
Kirkpatrick, J.D., Martin, E.C., Smart, R.L., et al., 2019, ApJS, 240, 19.
Leggett, S.K., et al., 2019, Astro 2020 Decadal White Paper "Discovery of Cold Brown Dwarfs or Free-floating Giant Planets Close to the Sun".
Leggett, S., Cushing, M., Hardegree-Ullman, K., et al. 2016, ApJ, 830, 141.
Luhman, K.L., 2014, ApJL, 786, L18.
Metchev, S, Heinze, A., Apai, D., et al. 2015, ApJ, 799, 154.
Metzger, B.D., & Pejcha, O., 2017, MNRAS, 471, 3200.
Morley, C., Fortney, J., Marley, M., et al. 2012, ApJ, 756, 172.
Reipurth, B., & Aspin, C., 2010, VAOA Conference, 19.
Robinson, T. & Marley, M., 2014, ApJ, 785, 158.
Schneider, A.C., Cushing, M.C., Kirkpatrick, J.D., et al., 2015, ApJ, 804, 92.
Vorobyov, E.I., & Basu, S., 2015, ApJ, 805, 115.
Wright, E.L., Mainzer, A., Kirkpatrick, J.D., et al., 2014, AJ, 148, 82.
Zhang, X. & Showman, A., 2014, ApJL, 788, L6.